Ordered chlorinated monolayer silicene structures

Wenbin Li,[1] Shaoxiang Sheng,[1] Jian Chen,[1] Peng Cheng,[1] Lan Chen,[1] and Kehui Wu[1,2,*]
[1]*Institute of Physics, Chinese Academy of Science, Beijing 100190, China*
[2]*Collaborative Innovation Center of Quantum Matter, Beijing 100871, China*
(Received 6 December 2015; revised manuscript received 22 February 2016; published 8 April 2016)

We report on a systematic experimental study on the chlorination of monatomic silicene layer on Ag(111) by scanning tunneling microscopy. Monolayer silicene on Ag(111) can form 4×4, ($\sqrt{13}\times\sqrt{13}$)R ± 13.9°, and ($2\sqrt{3}\times2\sqrt{3}$)R30° reconstructions due to their different buckling configurations. We found that at low dosage, Cl atoms attach to the upper buckled Si atoms without changing the buckling configuration of the silicene monolayer. However, at high coverage, the global buckling configuration will be significantly changed, resulting in new ordered structures. Interestingly, all monolayer silicene structures, regardless of their initial reconstructions, tend to form a local silicene 1×1 structure at the saturation coverage. The mechanism for chlorination of monolayer silicene is explained.

DOI: 10.1103/PhysRevB.93.155410

I. INTRODUCTION

Silicene, a honeycomb structure of silicon in analog to graphene, has been experimentally realized on a number of substrates, including Ag(111) [1–6], ZrB_2(0001) [7], Ir(111) [8], and MoS_2(0001) [9] in ultrahigh vacuum. Moreover, a demonstration of monolayer silicene device based on silicene grown on Ag(111) has been reported recently by Tao *et al.* [10]. However, there are still many challenging issues before any real device applications of silicene can be achieved. These include the search for nonmetallic substrates and solutions for surface protection and tuning the interaction between silicene and the substrate in order to preserve the Dirac electron state of pristine silicene. Other attractive topics in this field include multilayer silicene, which is expected to have better stability and chemical inertness than monolayer silicene [11–13]. In addition, germanene and stanene that are composed of other group-IV elements, Ge and Sn, have also attracted much attention recently [14–17]. These are expected to have increased spin-orbit-coupling strength and thus more intriguing spintronic properties.

For two-dimensional (2D) materials, an attractive feature is that all the atoms of the materials are exposed on the surface, and thus tuning the structure and properties by surface treatments becomes straightforward. For example, it has been reported that hydrogenation can induce gap opening at the Dirac point in graphene [18]. It is notable that in silicene, Si atoms have mixed sp^2/sp^3 hybridization; therefore the adsorption of foreign atoms on silicene would be easier to control than purely sp^2 hybridized graphene. There have been quite a number of theoretical studies on the hydrogenation and halogenation of silicene and germanene in the literature [19,20], while, experimentally, only the hydrogenation of silicene has been studied recently [21]. Compared with hydrogen, halogens interact with silicon more strongly; thus halogenation of monolayer silicene is expected to induce a larger gap and better inertness of the halogenated silicene in ambient condition [19,22,23]. Moreover, it is interesting that a recent theoretical work by Wang and Liu [24] indicated that halogenation of the Si(111) 7×7 surface into a $\sqrt{3}\times\sqrt{3}$ superlattice will generate a Dirac surface state. However, so far there has still been no experimental report on the halogenation of silicene.

In this work we report on a systematic scanning tunneling microscopy (STM) study on chlorination of monolayer silicene on Ag(111), with initial surface reconstructions including 4×4, ($\sqrt{13}\times\sqrt{13}$)R13.9°, and ($2\sqrt{3}\times2\sqrt{3}$)R30° phases, which are the most typical monolayer silicene phases found on Ag(111). We found that at low coverage, chlorine atoms adsorb on the upper buckled Si atoms without changing the buckling configuration of the silicene lattice, whereas at high coverage the buckling configuration will change, and new ordered structures as well as ordered defect patterns form. The models of these structures and defect patterns are explained in detail based on STM observations. Our work provides a comprehensive picture of silicene chlorination. The thus obtained chlorinated silicene, which can be regarded as 2D silicene derivatives, might be potentially useful to protect silicene or to tune the electronic state of silicene for device applications.

II. EXPERIMENTS

Our experiments were carried out in a home-built ultrahigh vacuum system (1×10^{-10} mbar) equipped with a low-temperature STM and a molecular beam epitaxy system. Single-crystal Ag(111) was used as the substrate. A clean Ag(111) surface was prepared by standard Ar^+ ion sputtering and annealing at 900 K. Si was deposited from a silicon wafer heated to about 1300 K. Monolayer silicene of different phases was prepared by depositing Si at different substrate temperatures. For example, coexisting 4×4 and ($\sqrt{13}\times\sqrt{13}$)R ± 13.9° phases were prepared at a substrate temperature of 470 K, while a pure ($2\sqrt{3}\times2\sqrt{3}$)R30° phase was prepared at 520 K. The chlorination of silicene was performed by exposing the samples to a Cl_2/Ar mixture gas (Cl_2/Ar = 2%, total pressure 2×10^{-3} Pa) at room temperature. Different exposure times were used for different Cl doses. In order to enhance the efficiency of chlorination, we also used a hot tungsten wire (about 2000 K) to crack the Cl_2 gas in some experiments. All our STM measurements were carried out at liquid-nitrogen

*khwu@iphy.ac.cn

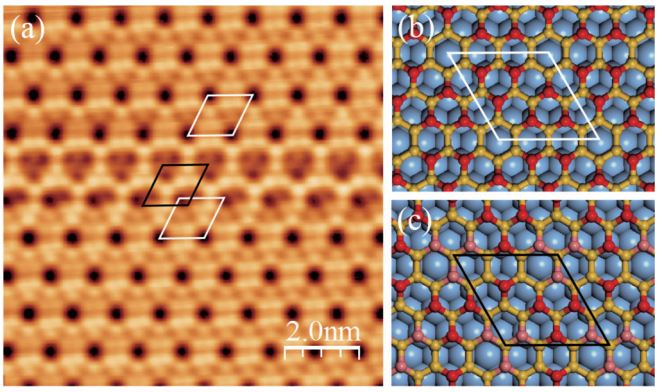

FIG. 1. STM image and models of silicene 4×4 phase on the Ag(111) surface. (a) Typical topography image of a clean silicene 4×4 surface (tip bias 100 mV, tunneling current 500 pA). The white rhombuses represent the unit cells of the α phase, and the black rhombus represents the unit cell of the β phase. Ball and stick models of the 4×4 (b) α and (c) β phases. The blue balls are silver atoms. The uppermost buckled Si atoms, upper buckled Si atoms, and the lower buckled Si atoms are represented by red, pink, and yellow balls, respectively.

temperature (77 K) in a constant current mode, with the bias voltage was applied to the tip.

III. RESULTS AND DISCUSSION

A. The 4×4 reconstruction

The 4×4 phase [with respect to Ag(111) 1×1] is the simplest phase among all monolayer silicene superstructures on Ag(111) [1]. The unit cell involves a 3×3 silicene supercell placed on the Ag(111) 4×4 supercell. There are two types of 4×4 phases, namely, α and β [25]. The α phase is the majority, whereas the β phase is the minority, found only around the boundaries between α domains. The structure models of α and β 4×4 are shown in Figs. 1(b) and 1(c), respectively. In each 4×4 unit cell of the α phase, there are two symmetric half unit cells (HUCs), each consisting of three upper buckled Si atoms. In contrast, in the 4×4 β phase the two HUCs are asymmetric, one with six upper buckled Si atoms and the other with only one upper buckled Si atom [25]. It should be emphasized that both the α and β phases correspond to the same silicene honeycomb lattice placed on top of Ag(111). The difference between them is simply due to different buckling configurations. It is known that in free-standing silicene, there are two sublattices, one consisting of upper buckled Si atoms and the other of lower buckled Si atoms. However, the buckling configuration will spontaneously rearrange once monolayer silicene is placed on a Ag(111) substrate. For example, in the 4×4 α phase the upper buckled Si atoms (red) in the two HUCs now belong to two different sublattices.

Figure 2(a) illustrates the result of chlorination of silicene 4×4 α at a small Cl dose. The basic feature of six spots in each 4×4 unit cell is preserved, while there appear individually very bright protrusions right on top of the original spots. The STM images give a straightforward picture of the Cl adsorption at low dosage: Cl atoms simply adsorbed on top of the upper buckled Si atoms without affecting the basic 4×4 silicene

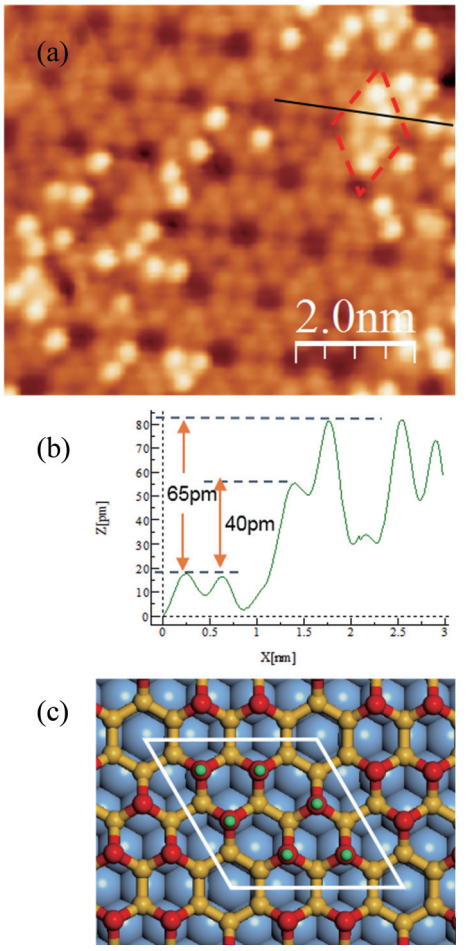

FIG. 2. STM image and structure model of the 4×4 α phase after chlorination with a small Cl dose. (a) Typical STM topography image of a 4×4 α phase with a small Cl dose (tip bias −100 mV, tunneling current −50 pA). (b) Height measurement along the black line in (a). (c) Model of Cl atoms adsorbed in a 4×4 α unit cell. The green balls represent possible Cl adsorption sites.

structure, as shown in Fig 2(c). The topographic height of the Cl atoms is 40-65 pm above the clean silicene surface, which shows very little change with tip bias ranging from 0.5 V to −0.6 V. However, the height measured by STM may be affected by the different electronic states on top of the Cl atom and on the Si atoms and does not necessarily correspond to the real height of the Cl atoms.

Increasing Cl atoms to a saturation dosage, we observed the transformation of the 4×4 α silicene to a flat surface containing ordered domains with different types of superstructures, as illustrated in Fig. 3. Several typical areas with ordered structures were highlighted by rectangles I-IV. The structures in areas I and II are similar to the fully hydrogenated silicene 4×4 structure reported previously: six bright spots in one HUC and one bright spot in another HUC [21]. In the case of hydrogenated silicene, the structure corresponds to the silicene 4×4 β structure with all the upper buckled Si atoms terminated by H atoms. The transformation from 4×4 α to 4×4 β upon hydrogenation is due to the H-induced strain effect [21]. We propose a similar structure model of the chlorinated silicene structures in I and II, as shown in Figs. 4(a) and 4(b),

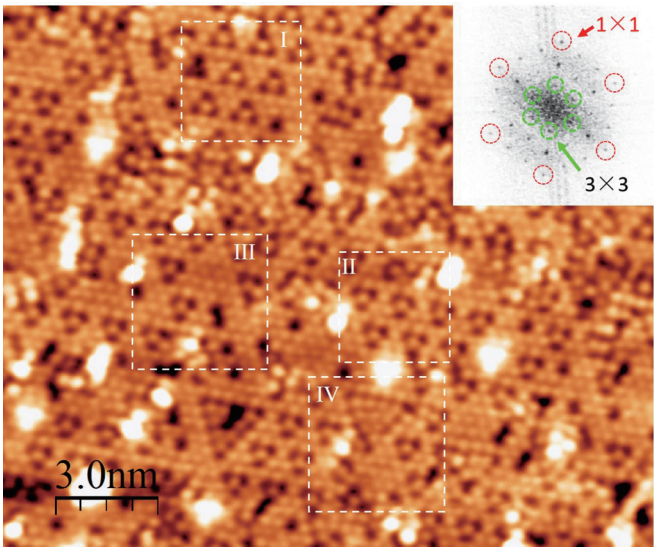

FIG. 3. Typical STM topographic image of fully chlorinated 4×4 phase (tip bias 1.50 V, tunneling current 20 pA). The inset is the FFT pattern of the STM image. The spots marked by red (green) circles are 1×1 (3×3) spots.

respectively. The configuration consists of six upper buckled Si atoms in in one HUC and one Si in another HUC, all of them terminated by Cl atoms. In another word, it is a silicene 4×4 β structure with all upper buckled Si atoms terminated by Cl atoms. It is noted that areas I and II correspond to the same structure, but the orientation of the triangular HUCs is flipped. This is because in 4×4 α silicene, the two HUCs are equivalent, with both having three upper buckled Si atoms. In contrast, in the 4×4 β phases the two HUCs become inequivalent. As a result, when the transformation from 4×4 α to the inequivalent 4×4 β occurs, there will be two possible configurations, which are mirror symmetric with respect to each other, as in areas I and II.

In areas III and IV, one observes local triangular domains consisting of close-packed protrusions in a 1×1 periodicity. Correspondingly, the fast Fourier transformation (FFT) of the STM image shows a sharp 1×1 pattern. The observation of a 1×1 structure indicates that the pristine silicene 1×1 lattice is recovered by Cl adsorption. In pristine silicene 1×1, one sublattice contains upper buckled Si, and the other contains lower buckled Si atoms. We propose that all the upper buckled Si atoms are terminated by Cl atoms, as illustrated in Fig. 4(c). Because during the transformation from 4×4 α to 1×1 the system can choose either one of the two sublattices as the upper buckled sublattice, there will also be two mirror-symmetric 1×1 domains. This is indeed observed in our experiment, as shown in Fig. 4(d). We found two triangular 1×1 domains, relatively shifted by half of the lattice constant of silicene 1×1, which is the lateral shift between the two sublattices.

The mobility of Cl atoms during the phase-transition process is an interesting issue. Initially, when the Cl coverage is low, they tend to adsorb individually on top of the upper buckled Si atoms in the 4×4 α unit cell. When all six upper buckled Si atoms in each 4×4 UC are terminated by Cl, further insertion of Cl atoms on the surface will cause the rearrangement of the buckling configuration, from six upper buckled Si atoms per UC (α phase) to seven upper buckled Si atoms per UC (β phase). Therefore one more Cl atom can be inserted on a 4×4 UC to reach the (almost) saturated Cl coverage. During this transition, some Cl atoms should adjust their adsorption sites. One can understand such mobility from two aspects: First, a Cl atom is only required to move to a neighboring Si atom, which is relatively easy since the Si-Si bond length is only 2.35 Å. [For comparison, in the case of Si(111) 7×7, the Cl atom is adsorbed on Si adatoms. The hopping of a Cl atom from one Si adatom to another Si adatom involves a distance of 11.9 Å, which is far more difficult.] Second, the movement of Cl atoms is accompanied by the change of buckling. Suppose there is an initially upper buckled Si atom with one Cl atom on top; when it becomes lower buckled, it spontaneously releases the Cl atom to its neighboring Si atom, which is now upper buckled. The hopping of the Cl atom may even gain energy from the lattice relaxation due to the rearrangement of buckling and may occur without much difficulty.

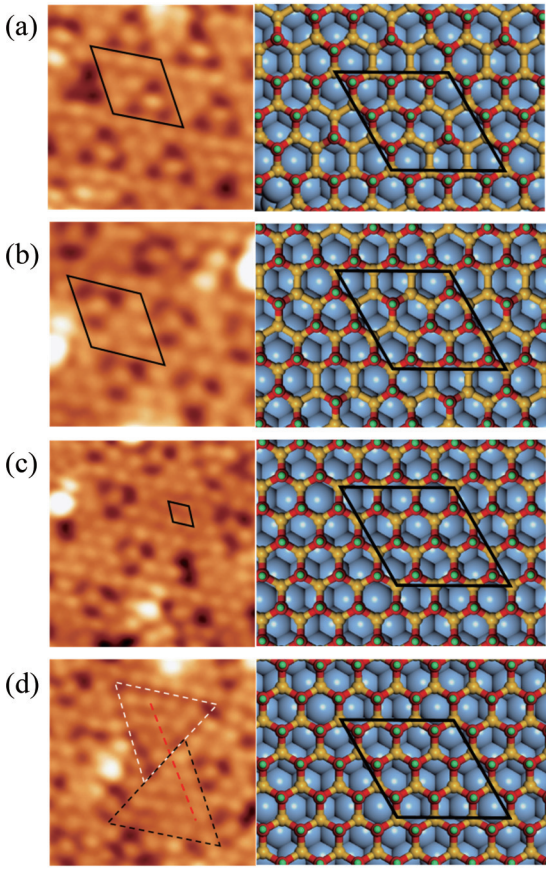

FIG. 4. Ordered structures in chlorinated silicene 4×4 surface. (a)–(d) Zoom in images of areas I-IV marked in Fig. 3 and the corresponding structure models. The right panels of (c) and (d) show two 1×1 models corresponding to two different upper buckled sublattices.

B. The $\sqrt{13}\times\sqrt{13}$ reconstruction

The second silicene phase studied for chlorination is the $(\sqrt{13}\times\sqrt{13})R\pm 13.9°$ phase [4,5], in which a silicene $\sqrt{7}\times\sqrt{7}$ supercell is superimposed on a Ag(111) $\sqrt{13}\times\sqrt{13}$ supercell,

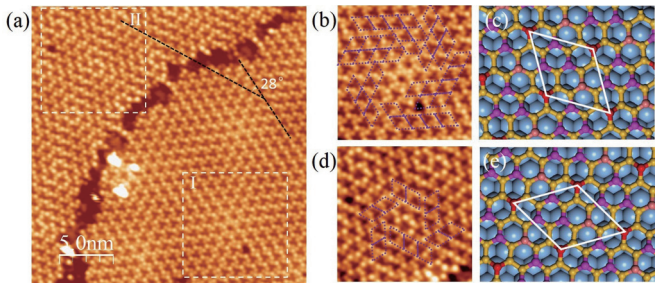

FIG. 5. ($\sqrt{13}\times\sqrt{13}$)R $\pm$ 13.9° reconstruction. (a) STM image of two typical domains of the ($\sqrt{13}\times\sqrt{13}$)R + 13.9° phase and ($\sqrt{13}\times\sqrt{13}$)R - 13.9°. The angle between their unit-cell directions is about 28° (tip bias 2.0 V, tunneling current 400 pA). (b) and (c) Enlarged image and model of area I in (a). (d) and (e) Enlarged STM image and model of area II in (a). The red, mauve, pink, and yellow atoms correspond to Si atoms with decreasing height. Purple dashed rhombuses in (b) and (d) and white rhombuses in (c) and (e) represent the $\sqrt{13}\times\sqrt{13}$ unit cells.

as shown in Fig. 5. In STM images, this phase shows vortexlike patterns with various vortex densities in different domains. Previous studies have suggested various atomic structure models of the $\sqrt{13}\times\sqrt{13}$ reconstruction [4–6,26,27], while recent work by Liu *et al.* gives a convincing picture of the atomic structure and vortexlike patterns of the $\sqrt{13}\times\sqrt{13}$ phase [25]. Figure 5(a) shows two typical $\sqrt{13}\times\sqrt{13}$ structures with different vortex patterns. Basically, the structure can be characterized by a vortex core surrounded by six triangular $\sqrt{13}\times\sqrt{13}$ domains. The unit-cell directions in neighboring domains are rotated by an angle of 60°. It should be emphasized again that the whole surface is a complete and continuous honeycomb silicene lattice. The appearance of these vortex pattern is solely due to the rearrangement of the buckling configuration of silicon atoms.

Figure 6(a) shows a typical STM image of the fully chlorinated silicene $\sqrt{13}\times\sqrt{13}$ phase. Two characteristic features can be revealed. First, the majority of the surface has been transformed into a close-packed 1×1 structure. Second, many defect sites occur on the surface. Interestingly, most defects are arranged periodically. The FFT of the STM image reveals both 1×1 and $\sqrt{7}\times\sqrt{7}$ patterns (with respect to silicene 1×1), corresponding to the 1×1 protrusions and periodically arranged defects. Most defects appear as a single dark site, which we call the monomer defect. There are also two-atom and three-atom defects, as marked in Fig. 6(d), which we refer to as dimer and trimer defects. In particular, the trimer defects are quite numerous on the surface, and they can be locally arranged in a compact $\sqrt{7}\times\sqrt{7}$ periodic pattern, as shown in Fig. 6(e). In the following we will discuss the 1×1 structure and the defects in detail.

The fact that the entire surface can be transformed to 1×1 proves that the $\sqrt{13}\times\sqrt{13}$ phase is a continuous silicene sheet. The vortex and domain structures in the original surface are only associated with buckling patterns, which can be rearranged to 1×1 by Cl adsorption. The atomic model of the chlorinated silicene 1×1 structure, including the Ag(111) substrate, is depicted in Fig. 6(f). Here the unit cell is marked as a white rhombus including a silicene $\sqrt{7}\times\sqrt{7}$ supercell overlapped by a Ag(111) $\sqrt{13}\times\sqrt{13}$ supercell. One of the

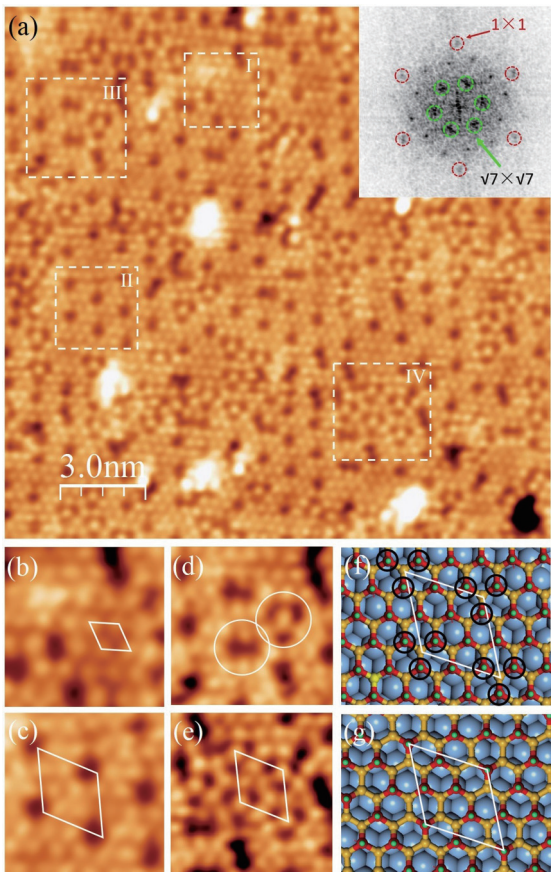

FIG. 6. Fully chlorinated silicene $\sqrt{13}\times\sqrt{13}$ phase. (a) Typical STM image of the $\sqrt{13}\times\sqrt{13}$ phase after fully chlorinated (tip bias 0.2 V, tunneling current 50 pA). The inset is the FFT of the image showing both 1×1 and $\sqrt{7}\times\sqrt{7}$ patterns (with respect to silicene 1×1). (b)-(e) Enlarged STM images of areas I-IV in (a). (f) Model of the silicene 1×1 structure in (b), with black circles corresponding to possible defect sites. (g) Structure model of trimer defects arranged in a $\sqrt{7}\times\sqrt{7}$ pattern (with respect to the silicene 1×1). The white rhombuses in (f) and (g) represent the unit cell of the $\sqrt{13}\times\sqrt{13}$ phase.

honeycomb sublattices, the red one in Fig. 6(f), is upper buckled. All the Si atoms in this sublattice are terminated by Cl atoms. Correspondingly, the yellow Si sublattice is lower buckled. It is noticed that at the corner of the rhombus unit cell, there is a lower buckled Si atom which sits right on top of an Ag atom. This Si atom should be less stable since it has a tendency to pop up. As a result, the three Si atoms surrounding the corner Si atom less readily adsorb Cl atoms on top. If one of the three Cl atoms is missing, there will be a monomer defect in this position, as shown in Fig. 6(c). This is the reason why monomer defects are arranged in a periodic $\sqrt{7}\times\sqrt{7}$ pattern. If two or three Cl atoms are missing, dimer or trimer defects will appear. Note that in the trimer-defect case, the corner Si atom pops up and becomes upper buckled, with one additional Cl atom adsorbed on top of it. As a result, the center of the trimer defect will become as bright as the other 1×1 Cl sites. The trimer defects are also arranged in a $\sqrt{7}\times\sqrt{7}$ pattern due to the position relation between silicene and the substrate, as shown in Fig. 6(e). We note that the monomer defects and

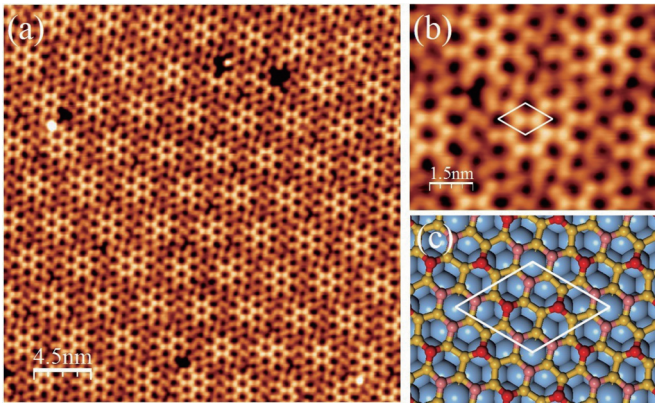

FIG. 7. Silicene $(2\sqrt{3}\times2\sqrt{3})$R30° phase. (a) Typical image of clean surface of $(2\sqrt{3}\times2\sqrt{3})$R30° phase (tip bias 1.0 V, tunneling current 500 pA). (b) Zoom-in image of the surface of (a); the rhombus represents the $2\sqrt{3}\times2\sqrt{3}$ unit cell. (c) Structural model of silicene $(2\sqrt{3}\times2\sqrt{3})$R30° phase. Atoms with red, pink, and yellow colors represent the uppermost buckled, the upper buckled, and the lower buckled Si atoms, respectively.

trimer defects are much more numerous than the dimer defects, which may be due to the better symmetry of the former two types of defects, which makes them energetically more stable.

C. The $2\sqrt{3}\times2\sqrt{3}$ reconstruction

The last silicene phase in our study of chlorination is $(2\sqrt{3}\times2\sqrt{3})$R30° [3,5], which involves a silicene $\sqrt{7}\times\sqrt{7}$ supercell placed on a Ag(111) $2\sqrt{3}\times2\sqrt{3}$ supercell, with a rotational angle of 30°, as shown in Fig. 7(c). Compared with 4×4 and $(\sqrt{13}\times\sqrt{13})$R $\pm$ 13.9°, $(2\sqrt{3}\times2\sqrt{3})$R30° is the most disordered and defective phase. The surface is characterized by a moiré-like pattern, as shown in Fig. 7(a) [3,28–30]. Each bright region consists of a few ordered hexagonal rings [Fig. 7(b)], corresponding to the $(2\sqrt{3}\times2\sqrt{3})$R30° superstructure, as depicted in Fig. 7(c). However, the regions between the bright regions appear defective and disordered, and the exact atomic structure model of these regions is still unclear. Different from the other phases which usually coexist with each other, the $(2\sqrt{3}\times2\sqrt{3})$R30° can exist as a single phase covering the entire Ag(111) substrate, and thus it is particularly interesting for possible device applications.

After chlorination at saturation Cl coverage, the surface transforms to a locally ordered silicene 1×1 structure, as shown in Fig. 8(a). This is similar to the hydrogenation of the silicene $(2\sqrt{3}\times2\sqrt{3})$R30° phase, which also results in an ordered silicene 1×1 [31]. The production of a pristine silicene 1×1 lattice by hydrogenation and chlorination proves that the original $(2\sqrt{3}\times2\sqrt{3})$R30° phase consists of a complete silicene honeycomb lattice. The apparent defective area in this phase is caused by the disorder in the buckling configuration instead of in the lattice.

Carefully inspecting the defect features, one can also distinguish three types of defects: monomer, dimer, and trimer, where the trimer defects appear as a regular triangle with a bright center. Moreover, a certain degree of ordering can be found in the arrangement of the defects, which can also be revealed by the FFT pattern, showing clear 1×1 and $\sqrt{7}\times\sqrt{7}$

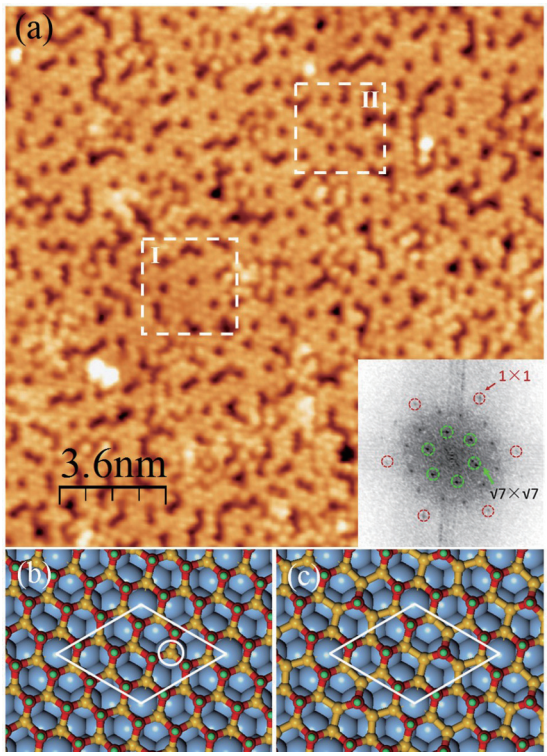

FIG. 8. Chlorinated silicene $2\sqrt{3}\times2\sqrt{3}$. (a) Typical STM image of chlorinated silicene $(2\sqrt{3}\times2\sqrt{3})$R30° (tip bias 0.6 V, tunneling current 50 pA). The inset is the FFT pattern of the image showing both 1×1 and $\sqrt{7}\times\sqrt{7}$ patterns (with respect to silicene 1×1). The areas marked as rectangles I and II includes typical monomer and trimer defects, respectively. (b) Model of fully chlorinated silicene 1×1 lattice. (c) Model of trimer defect lattice after chlorination.

patterns with respect to the silicene 1×1 lattice. We can understand the formation mechanism of these defects like in the $\sqrt{13}\times\sqrt{13}$ case. The atomic model of the chlorinated silicene 1×1 lattice was depicted in Fig. 8(b). One of the honeycomb sublattices, marked by red in Fig. 8(b), is upper buckled. All the Si atoms within this sublattice are terminated by Cl atoms and form a chlorinated silicene 1×1 lattice. Correspondingly, the other sublattice, marked by yellow, is lower buckled. It is noticed that in the unit cell, there is a lower buckled Si atom which sits right on top of a Ag atom [marked by the white circle in Fig. 8(b)]. This Si atom should be less stable in the lower buckled configuration since it has a tendency to pop up. As a result, there is a tendency for the three surrounding Si atoms to not adsorb a Cl atom since Cl adsorption would further increase the degree of buckling. Similar to those in the case of the $\sqrt{13}\times\sqrt{13}$ phase, the monomer, dimer, and trimer defects were generated when one, two, and three Cl atoms were missing, respectively.

It is also notable that although the chlorination of both silicene $\sqrt{13}\times\sqrt{13}$ and $2\sqrt{3}\times2\sqrt{3}$ results in 1×1 structures, the chlorinated $2\sqrt{3}\times2\sqrt{3}$ surface appears significantly more defective than the $\sqrt{13}\times\sqrt{13}$ case. The reason can be understood as follows. The adsorption of a Cl atom on top of an upper buckled Cl atom will pull the Si atom farther outward and thus increase its degree of buckling, similar to the adsorption of H on silicene [31]. As a result, adsorption of both H and

Cl will increase the compressive stress in the silicene film. On the other hand, the lattice mismatch between silicene and the Ag(111) substrate is different for different silicene phases. In the $2\sqrt{3}\times2\sqrt{3}$ phase, the silicene lattice is compressed, while in both 4×4 and $\sqrt{13}\times\sqrt{13}$ phases, the silicene 1×1 lattice is expanded by the Ag(111) substrate [the mismatch between lattice parameters: silicene $\sqrt{7}\times\sqrt{7}$/Ag(111) $2\sqrt{3}\times2\sqrt{3} \approx 1.02$, silicene $\sqrt{7}\times\sqrt{7}$/Ag(111) $\sqrt{13}\times\sqrt{13} \approx 0.98$, silicene 3×3/Ag(111) $4\times4 \approx 0.997$]. This means that the adsorption of Cl on 4×4 and $\sqrt{13}\times\sqrt{13}$ phases is preferable because it helps to compensate for the tensile stress and restore the silicene 1×1 lattice. In contrast, adsorption of Cl on silicene $2\sqrt{3}\times2\sqrt{3}$ would result in further compression of the silicene 1×1 lattice, thus making it more unstable. We suggest that this is the reason why the chlorinated $2\sqrt{3}\times2\sqrt{3}$ phase is more defective, with more missing Cl atoms.

Finally, we would like to compare the chlorination of silicene with the chlorination of the Si(111) 7×7 surface since the latter system has been well understood in the literature [32–34]. A common feature in both systems is the formation of the Cl-saturated, 1×1 surface structure. The main difference is that the Si(111) 7×7 reconstruction involves three atomic layers in a complex dimer-adatom-stacking fault (DAS) structure. The direct adsorption of Cl on Si(111) 7×7 will induce significant mass transport of Si atoms, including the breaking of the Si adatom back bonds [32]. The mass transport generally results in a rough surface instead of a well-defined Si(111) 1×1 Cl surface. Alternatively, a perfect Si(111) 1×1 Cl surface can be produced by a two-step process, which includes first obtaining a Si(111) 1×1 H surface by chemical wet etching and then replacing H with Cl by gas adsorption in UHV at room temperature [33]. This indicates that although the Si(111) 1×1 Cl is a stable phase, it is still important to control the dynamic process in order to achieve a perfect Si(111) 1×1 Cl surface. In contrast, in the case of silicene, all the Si atoms are located in a buckled honeycomb plane, and mass transport of Si atoms does not occur during Cl adsorption. This makes it a natural result to form a Cl-terminated 1×1 surface, similar to the chlorination of the hydrogen-terminated Si(111) 1×1 H surface.

In our experiment, we performed chlorination of the Si(111) 7×7 surface under the same conditions as for the chlorination of silicene. However, we found that chlorination of the Si(111) 7×7 surface under the same conditions usually results in a rough surface with only small pieces of Si(111) 1×1 Cl domains. In contrast, chlorination of silicene can result in a smooth surface with local 1×1 Cl domains. This demonstrates an obvious advantage of using silicene as the initial surface to produce functionalized silicene materials, for example, the possible Dirac surface state in halogenated Si(111) predicted by Wang and Liu [24]. The specific electronic structure of our chlorinated silicene is still under investigation.

IV. CONCLUSION

In summary, the chlorination of monolayer silicene with 4×4, $(\sqrt{13}\times\sqrt{13})$R $\pm$ 13.9°, and $(2\sqrt{3}\times2\sqrt{3})$R30° phases was systematically studied by STM. Chlorine atoms are found to adsorb on the top of the upper buckled Si atoms at low coverage, while at high coverage the global buckling configuration of silicene will be rearranged. After rearrangement the upper buckled Si atoms will be terminated by Cl atoms. It is interesting that at the saturation coverage, there is a trend to form locally a 1×1 lattice of pristine silicene regardless of the initial reconstruction of monolayer silicene. The thus obtained chlorinated silicene, as 2D silicene derivatives, may find future application in Si-based devices.

ACKNOWLEDGMENTS

This work was supported by the NSF of China (Grant No. 11334011), the MOST of China (Grants Nos. 2012CB921703, 2013CBA01601, 2013CB921702), and the Strategic Priority Research Program of the Chinese Academy of Sciences, Grant No. XDB07020100.

[1] P. Vogt, P. De Padova, C. Quaresima, J. Avila, E. Frantzeskakis, M. C. Asensio, A. Resta, B. Ealet, and G. Le Lay, Phys. Rev. Lett. **108**, 155501 (2012).
[2] L. Chen, C. C. Liu, B. J. Feng, X. Y. He, P. Cheng, Z. J. Ding, S. Meng, Y. G. Yao, and K. H. Wu, Phys. Rev. Lett. **109**, 056804 (2012).
[3] B. J. Feng, Z. J. Ding, S. Meng, Y. G. Yao, X. Y. He, P. Cheng, L. Chen, and K. H. Wu, Nano Lett. **12**, 3507 (2012).
[4] C. L. Lin, R. Arafune, K. Kawahara, N. Tsukahara, E. Minamitani, Y. Kim, N. Takagi, and M. Kawai, Appl. Phys. Express **5**, 045802 (2012).
[5] H. Jamgotchian, Y. Colignon, N. Hamzaoui, B. Ealet, J. Y. Hoarau, B. Aufray, and J. P. Biberian, J. Phys.: Condens. Matter **24**, 172001 (2012).
[6] H. Enriquez, S. Vizzini, A. Kara, B. Lalmi, and H. Oughaddou, J. Phys.: Condens. Matter **24**, 314211 (2012).
[7] A. Fleurence, R. Friedlein, T. Ozaki, H. Kawai, Y. Wang, and Y. Yamada-Takamura, Phys. Rev. Lett. **108**, 245501 (2012).
[8] L. Meng *et al.*, Nano Lett. **13**, 685 (2013).
[9] D. Chiappe, E. Scalise, E. Cinquanta, C. Grazianetti, B. van den Broek, M. Fanciulli, M. Houssa, and A. Molle, Adv. Mater. **26**, 2096 (2014).
[10] L. Tao, E. Cinquanta, D. Chiappe, C. Grazianetti, M. Fanciulli, M. Dubey, A. Molle, and D. Akinwande, Nat Nanotechnol. **10**, 227 (2015).
[11] P. De Padova *et al.*, Appl. Phys. Lett. **102**, 163106 (2013).
[12] J. Chen, Y. Du, Z. Li, W. B. Li, B. J. Feng, J. L. Qiu, P. Cheng, S. X. Dou, L. Chen, and K. H. Wu, Sci. Rep. **5**, 13590 (2015).
[13] R. Yaokawa, T. Ohsuna, T. Morishita, Y. Hayasaka, M. J. Spencer, and H. Nakano, Nat. Commun. **7**, 10657 (2016).
[14] M. Derivaz, D. Dentel, R. Stephan, M. C. Hanf, A. Mehdaoui, P. Sonnet, and C. Pirri, Nano Lett. **15**, 2510 (2015).
[15] L. Li, S. Z. Lu, J. Pan, Z. Qin, Y. Q. Wang, Y. Wang, G. Y. Cao, S. Du, and H. J. Gao, Adv. Mater. **26**, 4820 (2014).
[16] M. E. Davila, L. Xian, S. Cahangirov, A. Rubio, and G. Le Lay, New J. Phys. **16**, 095002 (2014).

[17] F. F. Zhu, W. J. Chen, Y. Xu, C. L. Gao, D. D. Guan, C. H. Liu, D. Qian, S. C. Zhang, and J. F. Jia, Nat. Mater. **14**, 1020 (2015).
[18] R. Balog *et al.*, Nat. Mater. **9**, 315 (2010).
[19] N. Gao, W. T. Zheng, and Q. Jiang, Phys. Chem. Chem. Phys. **14**, 257 (2012).
[20] P. Xiao, X.-L. Fan, and L.-M. Liu, Comput. Mater. Sci. **92**, 244 (2014).
[21] J. L. Qiu, H. X. Fu, Y. Xu, A. I. Oreshkin, T. N. Shao, H. Li, S. Meng, L. Chen, and K. H. Wu, Phys. Rev. Lett. **114**, 126101 (2015).
[22] L. C. Lew Yan Voon, E. Sandberg, R. S. Aga, and A. A. Farajian, Appl. Phys. Lett. **97**, 163114 (2010).
[23] B. Mohan, A. Kumar, and P. K. Ahluwalia, in *Solid State Physics: Proceedings of the 58th DAE Solid State Physics Symposium 2013*, AIP Conf. Proc. No. 1591 (AIP, New York, 2014), p. 1714.
[24] Z. F. Wang and F. Liu, Phys. Rev. Lett. **115**, 026803 (2015).
[25] Z. L. Liu, M. X. Wang, J. P. Xu, J. F. Ge, G. L. Lay, P. Vogt, D. Qian, C. L. Gao, C. Liu, and J. F. Jia, New J. Phys. **16**, 075006 (2014).
[26] Z.-X. Guo, S. Furuya, J.-I. Iwata, and A. Oshiyama, Phys. Rev. B **87**, 235435 (2013).
[27] J. Gao and J. Zhao, Sci. Rep. **2**, 861 (2012).
[28] H. Enriquez, A. Kara, A. J. Mayne, G. Dujardin, H. Jamgotchian, B. Aufray, and H. Oughaddou, J. Phys.: Conf. Ser. **491**, 012004 (2014).
[29] H. Jamgotchian, Y. Colignon, B. Ealet, B. Parditka, J.-Y. Hoarau, C. Girardeaux, B. Aufray, and J.-P. Bibérian, J. Phys.: Conf. Ser. **491**, 012001 (2014).
[30] Z. L. Liu, M. X. Wang, C. H. Liu, J. F. Jia, P. Vogt, C. Quaresima, C. Ottaviani, B. Olivieri, P. D. Padova, and G. L. Lay, APL Mater. **2**, 092513 (2014).
[31] J. L. Qiu, H. X. Fu, Y. Xu, Q. Zhou, S. Meng, H. Li, L. Chen, and K. H. Wu, ACS Nano **9**, 11192 (2015).
[32] J. J. Boland and J. S. Villarrubia, Science **248**, 838 (1990).
[33] B. J. Eves and G. P. Lopinski, Surf. Sci. **579**, 89 (2005).
[34] P. Maraghechi, S. A. Horn, and S. N. Patitsas, Surf. Sci. **601**, L1 (2007).